Journal of Material Sciences, Vol. 39 (2004) 2151-2157

HRTEM observation of the monoclinic-to-tetragonal (*m-t*) phase transition in nanocrystalline ZrO_2

I. Kasatkin[a,b*], F. Girgdies[a], T. Ressler[a], R.A. Caruso[c], J.H. Schattka[c], J. Urban[a], K.Weiss[a]

[a]Department of Inorganic Chemistry, Fritz-Haber-Institute of the MPG, Faradayweg 4-6, 14195 Berlin, Germany

[b]Department of Crystallography, Saint Petersburg State University, Universitetskaja, nab 7/9, 199034 Saint-Petersburg, Russian Federation

[c]Max Planck Institute of Colloids and Interfaces, 14434 Potsdam, Germany

[*] Corresponding author: e-mail kasatki@fhi-berlin.mpg.de

Abstract

The orientation relations *m*(100) || *t*(001), *m*[001] || *t*[110]; *m*(011) || *t*(100), *m*[100] || *t*[001]; *m*(100) || *t*(110), *m*[001] || *t*[001]; *m*(013) || *t*(116), *m*[001] || *t*[001] (indices for the primitive tetragonal cell) have been found between the tetragonal (*t*) and monoclinic (*m*) domains during the electron irradiation-induced *m-t* phase transition observed in-situ with HREM within isolated zirconia nanoparticles. Geometric models of the *m-t* interfaces are proposed.

Keywords:

High-resolution transmission electron microscopy, nanoparticles, orientation relations, polymorphism, zirconia, catalyst

1.Introduction

Copper based catalysts can be used for reactions such as water-gas shift, methanol synthesis, and methanol steam reforming. Some investigations have recently been done on catalysts containing both copper and ZrO_2 (zirconia) with respect to the above reactions. In this context, the zirconia may be used either as a stabilizing additive to the $Cu/ZnO(/Al_2O_3)$ catalysts [1], or as an alternative support replacing for example, ZnO [2]. Zirconia modified with anions such as sulphate is an acid catalyst and became known for its extraordinary activity in low-temperature alkane isomerization [3]; it is also active for a number of other acid-catalysed reactions [4].

In this work Cu oxide supported on zirconium dioxide was characterized with high-resolution transmission electron microscopy (HRTEM), and polymorphic phase transitions observed in ZrO_2 are reported.

Polymorphism of zirconia has been excessively studied during the past several decades on both the macro- and microscale with the use of a wide variety of experimental techniques. The sequence of thermodynamically stable polymorphs into which crystalline ZrO_2 reversibly transforms on heating at atmospheric pressure is now firmly established for bulk material and is: $m - t - c$ (here and below the indices *m, t, c* stand for the monoclinic, tetragonal and the cubic phase, correspondingly). But when the powders of unstabilized or partially stabilized (by additives) zirconia are obtained by thermal treatment of amorphous precursors the *t*-phase appears first, at lower temperature, and then it transforms into *m*-phase as the temperature rises [5 – 7]. The reasons of this phenomenon have been (and still are) the object of numerous discussions in the literature. The appearance of the tetragonal phase was attributed to the similarity of its structure to that of amorphous (hydrous) ZrO_2, which makes the crystallization of *t*-zirconia kinetically preferable [7].

For dispersed nanocrystalline materials consisting of unconstrained particles below a certain critical size the excess of surface energy may be sufficient for stabilizing those modifications, which would be unstable for the bulk material at the same conditions [8, 9]. This applies to ZrO_2 whose *t*-phase has a lower surface energy than the *m*-phase [10, 11], and different authors theoretically estimated the critical size of a strain-free crystal as 5 nm [9] or 7 nm [12]. However, experimentally determined critical diameters were invariably higher than the estimates: 18 nm [12], 10-40 nm [13]. It should be noted that surface adsorption of water [14] or of other species may alter the energetic considerations.

Smaller particles also have higher internal pressure due to surface curvature (the Gibbs-Thomson effect). This is considered as another possible mechanism of stabilization of high-temperature and high-pressure polymorphs by the small crystallite size [15, 16]. In the recent publications the size-effect is mentioned among the main reasons of the *t*-phase stabilisation for unconstrained zirconia nanoparticles having no strong interaction with a support [13, 17 - 25]. Anionic vacancies [26, 27] and domain boundaries [28] may also be responsible for the *t*-phase stabilization at the ambient temperatures. In many papers the effect of stress on the

Table 1. Orientation relations between the tetragonal and monoclinic phases of ZrO_2.

Ref.	N		Orientation relations I : conventional tetragonal cell (primitive)		Orientation relations II : double tetragonal cell (base-centered, $\mathbf{a}^{II}=\mathbf{a}_1^{I}+\mathbf{a}_2^{I}$)		Habit plane
[31]	1	a	*m*[001] || *t*[001]	*m*(100) || *t*(110)	***m*[001] || *t*[001]**	***m*(100) || *t*(100)**	
		b	*m*[001] || *t*[110]	*m*(100) || *t*(001)	***m*[001] || *t*[100]**	***m*(100) || *t*(001)**	
		c	*m*[001] || *t*[110]	*m*(100) || *t*(110)	***m*[001] || *t*[100]**	***m*(100) || *t*(100)**	
[32]	2	a	*m*[010] || *t*[110]	*m*(101) || *t*(111)	***m*[010] || *t*[010]**	***m*(101) || *t*(101)**	
		b	*m*[010] || *t*[001]	*m*(101) || *t*(100)	***m*[010] || *t*[001]**	***m*(101) || *t*(110)**	
[33]	3		***m*[001] || *t*[001]**	***m*(100) || *t*(110)**	*m*[001] || *t*[001]	*m*(100) || *t*(100)	
[34]	4		*m*[010] || *t*[001]	*m*(100) || *t*(110)	***m*[010] || *t*[001]**	***m*(100) || *t*(100)**	
[35]	5	a	***m*[010] || t[001]**	***m*(100) || *t*(110)**	*m*[010] || t[001]	*m*(100) || *t*(100)	*m*(100)
		b	***m*[001] || *t*[001]**	***m*(100) || *t*(110)**	*m*[001] || *t*[001]	*m*(100) || *t*(100)	
[36]	6	a	*m*[100] || *t*[110]	*m*(001) || *t*(001)	***m*[100] || *t*[100]**	***m*(001) || *t*(001)**	*m*(001)
		b	*m*[001] || *t*[001]	*m*(100) || *t*(110)	***m*[001] || *t*[001]**	***m*(100) || *t*(100)**	*m*(100)
[37]	7	a	*m*[100] || *t*[110]	*m*(001) || *t*(110)	***m*[100] || *t*[100]**	***m*(001) || *t*(100)**	*m*(671), *m*(761), *m*~(100), *m*~(010)
		b	*m*[001] || *t*[110]	*m*(100) || *t*(110)	***m*[001] || *t*[100]**	***m*(100) || *t*(100)**	
		c	*m*[001] || *t*[001]	*m*(100) || *t*(110)	***m*[001] || *t*[001]**	***m*(100) || *t*(100)**	
[38]	8	a	*m*[001] || *t*[110]	*m*(100) || *t*(-110)	***m*[001] || *t*[100]**	***m*(100) || *t*(010)**	
		b	*m*[100] || *t*[-110]	*m*(001) || *t*(110)	***m*[100] || *t*[010]**	***m*(001) || *t*(100)**	
		c	*m*[001] || *t*[001]	*m*(100) || *t*(-110)	***m*[001] || *t*[001]**	***m*(100) || *t*(010)**	
[39]	9		***m*[1-10] || *t*[100]**	***m*(001) || *t*(001)**	*m*[100] || *t*[100]	*m*(001) || *t*(001)	*m*(671) *m*(111) = *t*(01-1)
[40]	10		***m*[001] || *t*[001]**	***m*(100) || *t*(110)**	*m*[001] || *t*[001]	*m*(100) || *t*(100)	*m*(100) = *t*(110)
[41]	11		**?**	***m*(111) || *t*(101)**	?	*m*(111) || *t*(111)	*m*(111) = *t*(101)

t-m transformation occurring in both the dispersed powders and sintered ceramics has been reported. These are not addressed here.

In this paper a relatively rare monoclinic-to-tetragonal, *m-t* (and not the commonly observed tetragonal-to-monoclinic, *t-m*) electron beam-induced phase transition in isolated unconstrained nanoparticles of ZrO_2 occurring at the temperature below the corresponding transition temperature known for the bulk material (about 1200 ^oC) is described. Earlier this type of transition has been observed on heating the undoped *m*-ZrO_2 nanopowder [29] and interpreted as a manifestation of the true thermodynamic stability of nanoscale (particle size ≤ 20 nm) *t*-zirconia at the temperatures between 900 and 1100 ^oC. Irradiation by 800 keV Bi ions was also shown to cause the *m-t* transition [30] in a coarse-grained pure material (particle size about 10 μm) at room temperature due to the strains caused by irradiation-induced defects. At the same time, the irradiation with 2.5 MeV electrons did not produce any phase changes in the material [30].

Irrespective of the crystal size, the problem of orientation relations between the domains of different phases within a zirconia crystal undergoing the transition or between the grains within ceramic materials attracted considerable attention. Table 1 summarizes the data available in the literature.

The authors of [31, 32, 34, 36-38] used the base-centered tetragonal cell (face-centered if only the Zr-sublattice is considered), which is doubled with respect to the conventional cell. In Table 1 the orientation relations are presented for both the cell choices (in bold are shown the relations as they appeared in the original papers; the conversion of indices into the other setting was done by us). From [39] it was unclear which cell was used for indexing, but the lattice correspondence (habit plane) suggested that it was the conventional cell. In the present work all the indexing is done for the conventional primitive tetragonal cell (body-centered for Zr-sublattice).

Among the orientation relations listed in the Table 1 there are only nine principally different variants, say, 1a, 1b, 1c, 2a, 2b, 6a, 7a, and 9. The others are just different formulations of the same relations: 3 = 5b = 6b = 7c = 8c = 10 = 1a; 4 = 5a = 7b = 8a = 1c; 8b = 7a; 11 = 9 (seemingly). The existence of the relation 1b have not been proved experimentally. Moreover, it should be noted that the tetragonal structure of zirconia differs only slightly from the fluorite-type cubic structure. Because of this fact experimental difficulties arise in distinguishing between the tetragonal and cubic phases or between certain orientations of the tetragonal phase by diffraction data [31].

2. Experimental

2.1. Material preparation

A templating procedure [42] was used for the synthesis of the CuO/ZrO_2 material, which involved the use of a polymer gel template [43]. This particular template was an acrylamide/glycidyl methacrylate polymer formed in an aqueous Tween-60 (Aldrich) solution at 55 °C. After cleaning and solvent exchange to n-propanol the gel was soaked in a zirconium (IV) propoxide (Aldrich, 70 % by mass in n-propanol) solution containing copper(II) acetylacetonate (Aldrich, 2.0 g) for 16 h to give theoretically an 11 % Cu to Cu+Zr mass ratio. The impregnated gel was then placed into a mixture of n-propanol/water (1:1 v/v) and left overnight during which hydrolysis reactions occurred. The hybrid material was dried at room temperature open to the atmosphere, and then calcined at 450 °C (ramp 215 $°C \cdot h^{-1}$) under a nitrogen then oxygen atmosphere to remove the organic material.

From the X-ray powder diffractogram with broad reflections taken after the calcination procedure it was hardly possible to estimate the tetragonal-to-monoclinic ratio for crystalline zirconia accurately, but it may be assumed that the content of *m*-ZrO_2 was less than 10 % vol. No peaks of Cu or Cu oxides were seen. Then the powder was heated with the rate of 5 °C per hour up to 250 ^oC and kept for 10 h at that temperature under normal pressure in a helium atmosphere containing 2 % of hydrogen in an in-situ camera attached to X-ray diffractometer. A small peak of metallic copper appeared (the content of Cu was estimated as ~ 6 % vol.) and the content of *m*-ZrO_2 did not change considerably. The resulting powder had been kept in a hermetically closed vessel under 1 atm Ar pressure during two weeks before it was studied with HRTEM.

2.2. HRTEM study

The material was dispersed in acetone, sonicated for 10 min. and deposited on a copper grid covered with an amorphous carbon film of about 5 nm thickness. A Philips CM200FEG microscope, 200 kV, equipped with a field emission gun was used. The coefficient of spherical aberration was C_s = 1.35 mm. The information limit was better than 0.18 nm. High-resolution images with a pixel size of 0.044 nm were taken at the magnification of 1083000× with a CCD camera and processed to obtain the power spectra (square of the Fourier transform of the image). The power spectra (PS) were used for measuring interplanar distances and angles. The former were measured within the accuracy of ± 1 %, the latter ± 0.5 deg.

Energy dispersive X-ray spectroscopy (EDX) was used for the determination of the average composition of the sample and for the elemental mapping. For this purpose other samples were prepared using nickel grids.

3. Results

The mean particle size measured in the HRTEM images and that obtained from the analysis of XRD line broadening with the use of Scherrer formula were in a good agreement: 8.6 nm and 8.3 nm, respectively. This means that during the ultrasonic treatment of the powder disintegration of the particles did not occur. It should be noted,

however, that within the same sample much larger single particles with sizes above 20 nm were sometimes microscopically observed but not included in the above statistics.

The quantitative EDX analysis gave the following average composition: Zr – 33 ± 3.9 at %; Cu – 7.4 ± 0.3 at %; O – 59.6 ± 1.3 at %. The elemental mapping showed a more or less homogeneous distribution of Cu in the sample (no Cu or Cu oxide particles bigger than 20 nm). Several nanoparticles (5-15 nm in size) were found, which were recognized as those of cuprite (Cu_2O), paramelaconite (Cu_4O_3), tenorite (CuO), and metallic Cu.

Analysis of X-ray diffraction diagrams taken for a series of samples revealed no correlation between the overall Cu content and lattice constants of zirconia, which would indicate a substitution of Zr^{4+} by Cu^{2+} in its structure.

In Fig. 1 the electron diffraction (ED) profile is compared to that obtained with XRD. It is seen that ED (pattern taken 1 hour after the sample had been put in the column of the electron microscope) showed much higher content of *m*-ZrO_2, but *t*-ZrO_2 was still the dominating phase.

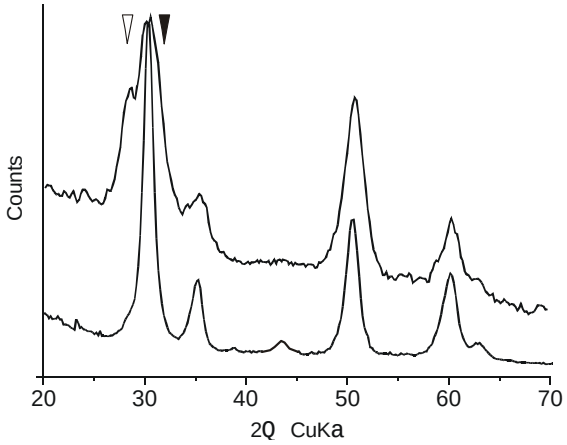

Fig. 1. Profiles of X-ray diffraction (lower curve) and electron diffraction (upper curve). The positions of the $\bar{1}11$ and 111 peaks of *m*-ZrO_2 are marked with the open and filled triangles, correspondingly.

Among the zirconia particles whose structure could be unambiguously identified in the HRTEM images, about 60 % were monoclinic and only 40 % tetragonal. The mean size (the diameter of a circle having the same area as the particle) of the tetragonal particles was 7.4 nm and that of the monoclinic ones – 9.2 nm. At the same time, X-ray powder diffractogram taken from the rest of the sample prepared for the HRTEM study showed no noticeable changes in the tetragonal-to-monoclinic ratio. This disproves the possibility of the $t \rightarrow m$ transition occurring during the time of keeping and/or sonication of the material. A transition induced by the electron irradiation under high-vacuum conditions should be considered as the only possible explanation of the discrepancy.

Fig. 2a shows a particle of *m*-ZrO_2 viewed along the [0 1 $\bar{1}$] direction, the indexed PS of the particle image (Fig. 2b), and the filtered image obtained by an inverse Fourier transformation after subtraction of the background and the central spot removal from the PS (Fig. 2c). The interplanar distances measured in the PS for the four spots closest to the centre were: 0.51, 0.364, 0.307, and 0.283 nm. They correspond to d_{100} = 0.509 nm, d_{011} = 0.370 nm, $d_{\bar{1}11}$ = 0.316 nm, and d_{111} = 0.284 nm in *m*-ZrO_2 [44]. The angles were: 83.0 deg between the planes (100) and (011), and 71.0 deg between (111) and ($\bar{1}$11), which corresponded within ± 1 deg to those in monoclinic zirconia: 83.5 and 72.0 deg (calculated from the data given in [45]).

In Fig. 2d the same particle is shown after 3 min of irradiation by the electron beam. It is seen that about 1/3 of its volume has become tetragonal with [1 $\bar{1}$ $\bar{1}$] parallel to the viewing direction. This conclusion was confirmed by the distances and angles measured in the PS shown in Fig. 2e: 0.296 nm (with the angle of 70.2 deg between the equivalent planes), 0.254, and 0.183 nm, which were very close to those in *t*-ZrO_2: d_{101} = 0.295 (the angle between (101) and (011) is 71.0 deg) nm, d_{110} = 0.254 nm, d_{112} = 0.181 nm (calculated from the structural data given in [45]). At the same time the rest of the particle remained monoclinic with nearly the same orientation as before. From the power spectra shown in Fig. 2b and Fig. 2e it follows that the "habit plane" (the plane that is common for both the phases) is (110) for tetragonal and (100) for monoclinic zirconia.

Due to the similar values of d_{110} = 0.254 nm ≈ d_{002} = 0.258 nm and d_{112} = 0.181 nm ≈ d_{200} = 0.180 nm in the tetragonal structure [45] the orientation determined here as [1 $\bar{1}$ $\bar{1}$] could also be described as [100]. To distinguish between these two orientations we used the ratio of d-spacings: d_{112} / d_{110} = 0.715 ± 0.008 (d_{112} / d_{110} = 0.712 in the ideal structure). For the [100] orientation the corresponding ratio should be close to d_{200} / d_{002} = 0.696.

Fig. 3 shows two examples of the composite particles consisting of monoclinic and tetragonal parts. In both cases the [010] directions of the tetragonal domains were oriented along the viewing direction. The ratios of the d-spacings were d_{200} / d_{002} = 0.697 ± 0.008 and d_{200} / d_{002} = 0.694 ± 0.008 for the particles shown in Fig. 3a and Fig. 3d, respectively. In the particle shown in Fig. 3a a "core-shell" relationship exist between the monoclinic and tetragonal parts. Correspondingly, two different habit planes can be distinguished: *m*(100) ∥ *t*(001) projected approximately along the line shown with two white arrows, and *m*(011) ∥ *t*(100) indicated with black arrows. The orientation relation can be described as *m*[001] ∥ *t*[110]. This relation is incompatible with *m*(011) ∥ *t*(100), and it should better be formulated as *m*[100] ∥ *t*[001] for the latter case. These two slightly different relations can coexist in a single particle only if both the structures (or, at least, one of them) are distorted. Fig 3a shows that the (10 $\bar{1}$) lattice planes are bent. This is, probably, the result of the accommodating distortion.

In Fig. 4a a similar "core-shell" structure is seen in a different projection: along [031] for the monoclinic core and along [331] for the tetragonal shell. The ratio of the d-spacings corresponding to the weak and to the strong reflections in the PS of the tetragonal part was determined as

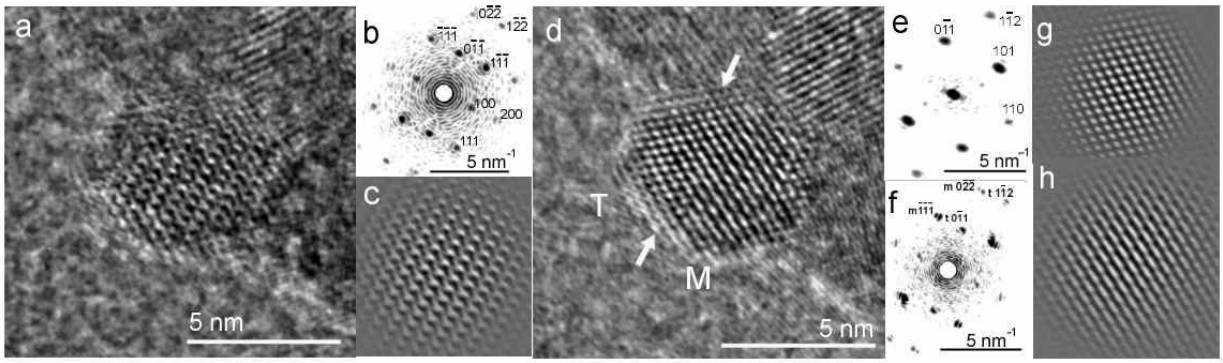

Fig. 2. a) HRTEM image of a m-ZrO_2 particle viewed along [0 1 $\bar{1}$]; b) PS of the image of a); c) filtered image of a); d) the same particle after 3 min of electron beam irradiation; arrows point to the boundary between t- and m-phases of ZrO_2; viewing direction for t-ZrO_2 is [1 $\bar{1}$ $\bar{1}$]; e), f) PS of tetragonal and monoclinic parts, respectively; g), h) filtered images of t- and m- parts, respectively. Filtered images have the same scale as the original ones.

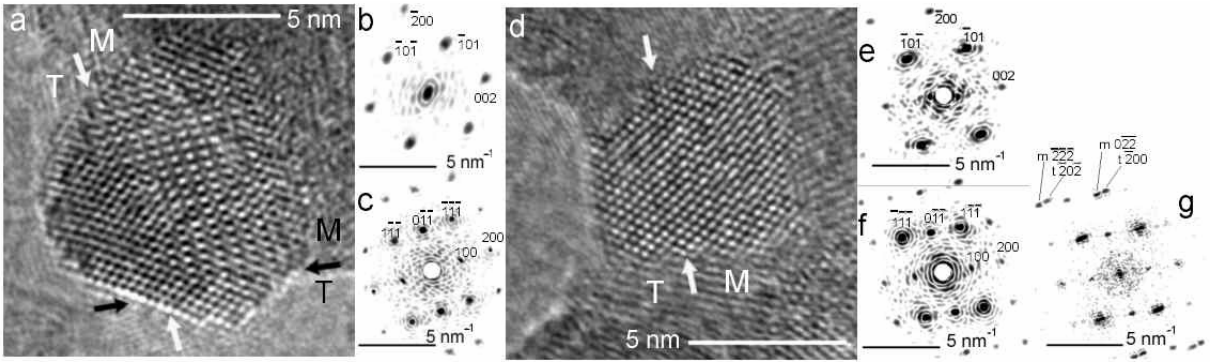

Fig. 3. a), d) HRTEM images of composite particles consisting of m-ZrO_2 (viewing direction [0 1 $\bar{1}$]) and t-ZrO_2 (viewing direction [010]); white and black arrows point to the boundaries between t- and m-phases; b) PS of the tetragonal part of a); c) PS of the monoclinic part of a); e) PS of the tetragonal part of d); f) PS of the monoclinic part of d); g) PS of the whole particle of d).

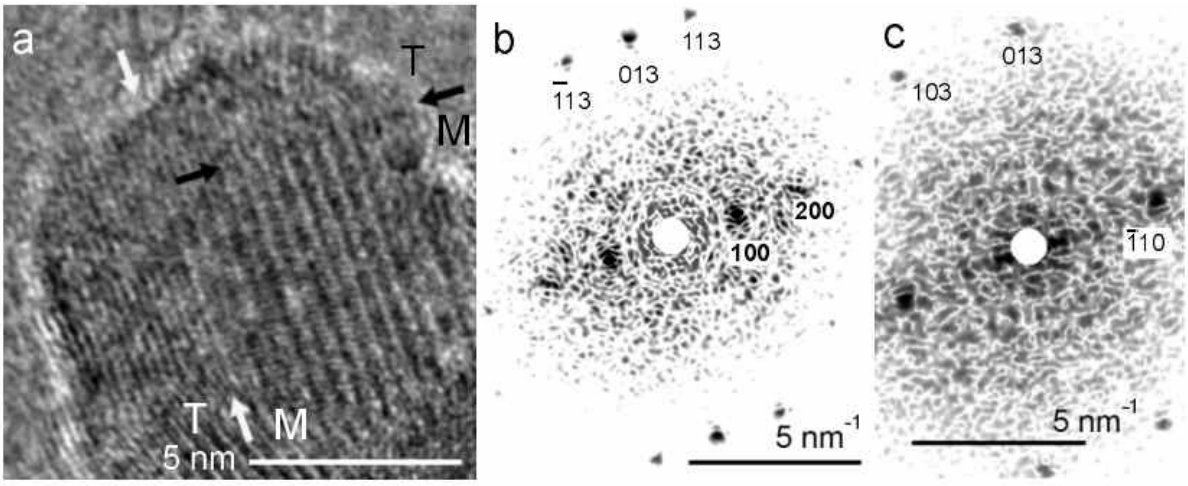

Fig. 4. a) composite particle showing a “core-shell” relationship between the m- (“core”, viewing direction [031]) and t- parts (“shell”, viewing direction [331]); b), c) PS of the monoclinic and tetragonal parts, respectively.

0.612 ± 0.007 (≈ d_{103} / d_{110} = 0.610) that suggested the orientation to be || [331] rather than || [120] (d_{211} / d_{002} = 0.595). The orientation relation may be written as *m*[001] || *t*[001], which is the same as that shown in Fig. 2. The habit plane shown with the white arrows is again (100) for the monoclinic part and (110) for the tetragonal one. With the

black arrows in Fig. 4a is shown another habit plane: *m*(013) and *t*(116).

It is seen in the images of Fig. 2 and Fig. 3 that the *t*-*m* interface is coherent and certain lattice planes cross it nearly undisturbed. These are the ($\bar{1}$ 1 1), (111), and (011) planes in the monoclinic modification which become the (101) and (112) (Fig. 2), or (101) and (100) (Fig. 3) planes in the tetragonal part of the particle. A closer look at the images reveals that the planes change their direction slightly at the interface (the measured angles were in the range of 4 - 5.5 deg. for different particles); the effect is best seen if an image is viewed in a perspective. The change in orientation explains the splitting of maxima in the PS shown in Fig. 3g (the PS taken from the whole of the particle in Fig. 3d) and itself is explained by the difference of about 5 deg. in the inclination of these planes to the habit plane in the ideal structures of *m*- and *t*-ZrO_2.

The curvature of the *m*(100) and *t*(110) (Fig. 2b) or *t*(001) (Fig. 3a) planes at the interface is, probably, due to strain caused by the difference in the interplanar distances of *m*-$d_{\bar{1}11}$ = 0.316 nm and *t*-d_{101} = 0.294 nm. In a bulk crystal such a misfit should cause compensating dislocations to appear. A simple calculation (*m*-$d_{\bar{1}11}$) / (*m*-$d_{\bar{1}11}$ − *t*-d_{101}) shows that a dislocation should be produced on the interface for every 14 ($\bar{1}$ 1 1) planes in the monoclinic phase which corresponds to the distance of about 4.5 nm. In Fig. 2b and Fig. 3a it is seen that the particles are about of the critical size for the appearance of dislocations. Surprisingly, the lattice planes appear straight in the image of Fig. 3d.

Thus, the orientation relations between the monoclinic and tetragonal domains observed in this work can be formulated as follows:

m(100) || *t*(110); (1)
m[001] || *t*[001]

m(013) || *t*(116); (2)
m[001] || *t*[001]

m(100) || *t*(001); (3)
m[001] || *t*[110]

m(011) || *t*(100); (4)
m[100] || *t*[001].

Among the listed only the relation (1) has been observed experimentally earlier [31, 33, 35-38]. The relation (3) has been suggested by Bailey [31], but no experimental evidence of its existence has been reported.

4. Discussion

From the relations described above a geometrical model of the *t*-*m* interface can be derived. Fig. 5 shows the projections of the tetragonal and the monoclinic structures onto the habit planes for the orientation relations (1) and (3). It is seen that the atomic arrangements within these planes are very similar in both the structures, albeit in the [100] plane of the monoclinic structure and in the [110]

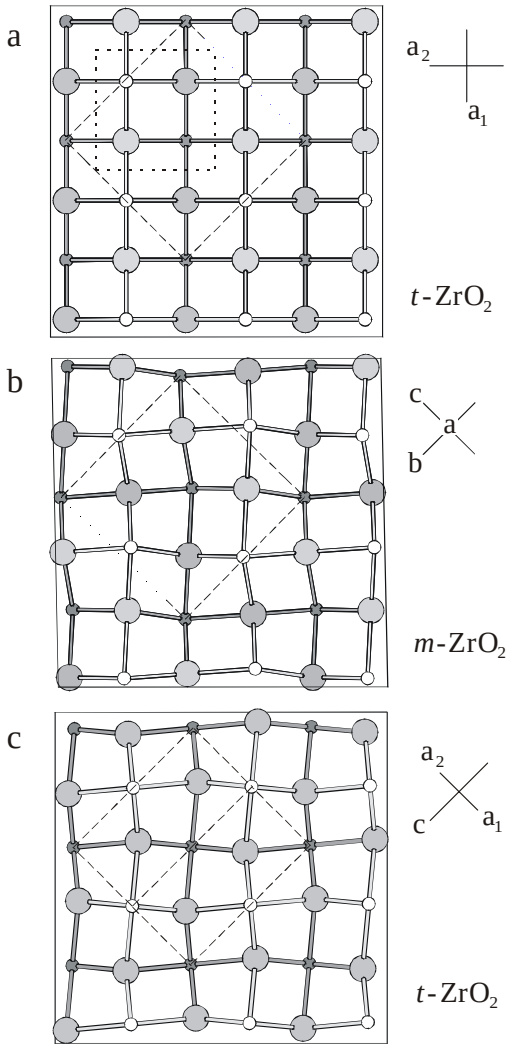

Fig. 5. Lattice planes matched (habit planes) in the case of orientation relations (1) and (3) in the tetragonal (a, c) and monoclinic (b) structures of ZrO_2: (100) plane of m- ZrO_2 (b), (001) (a) and (110) (c) planes for t-ZrO_2. Dashed lines – projections of the corresponding unit cells (for t-ZrO_2 – of the base-centered C-cell); dotted line in a) – projection of the conventional P-cell). Small circles – Zr, large circles – O; shade shows the depth.

plane of the tetragonal one there exist small displacements of the atoms from those lattice points, which they would occupy in the corresponding planes of the fluorite structure. From a comparison of the projections the atom movements necessary to accommodate the misfit and to keep the coherency of the interface are immediately obvious.

In Fig. 6 the interfaces between the two phases are depicted in the same orientations as in the HRTEM images of Fig. 2d, Fig. 3a, and Fig. 3d. Black circles show the Zr atoms, which belong to both the phases simultaneously. It is seen that the coordination polyhedra for those atoms that form the interface are nearly the same as the slightly distorted cubes in the tetragonal structure, but the degree of distortion is higher.

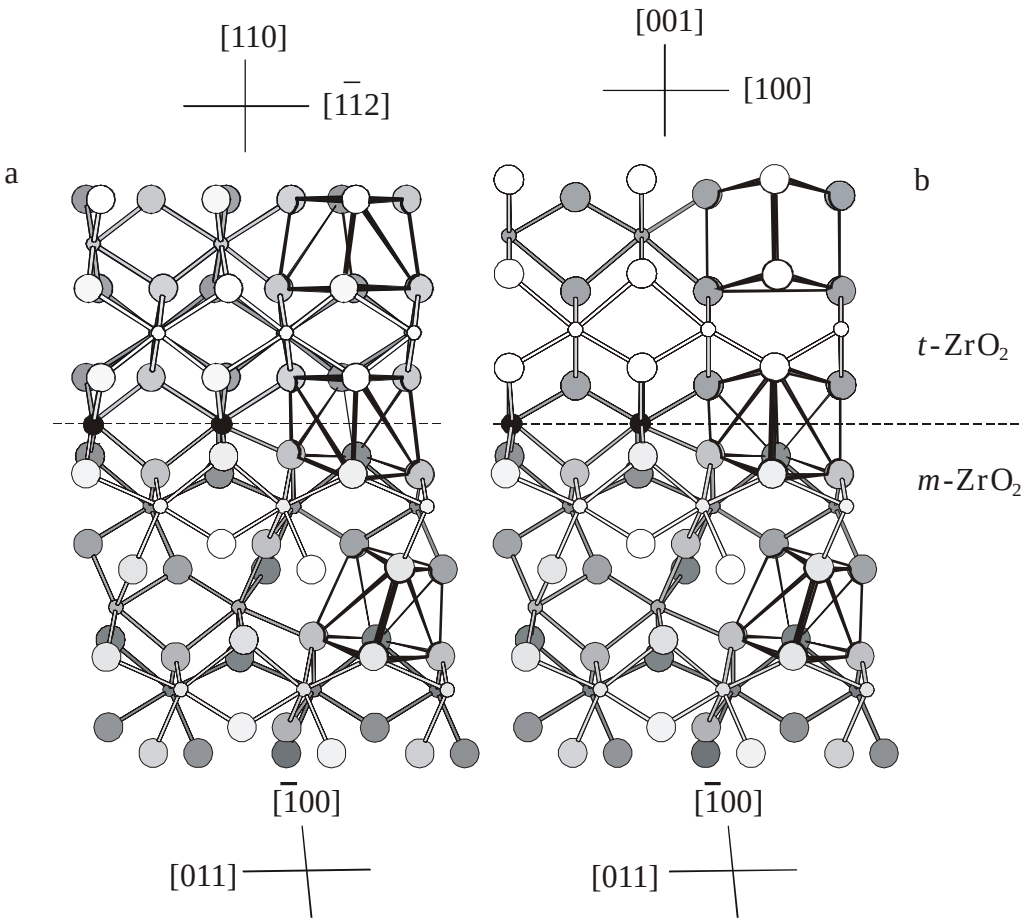

Fig. 6. Models of the *t*-*m* interfaces for the orientation relations (1) and (3). a) Projection corresponds to that in Fig. 2d; b) projection corresponds to that in Fig. 3a, 3d. Small circles – Zr, large circles – O; shade shows the depth; black circles – Zr atoms belonging to the interface. The coordination polyhedra are shown without the central Zr atoms.

The lattice planes corresponding to the habit planes for the relations (2) and (4) are shown in Fig. 7. It is seen that the orthogonal lattices in the tetragonal structure should be matched with the non-orthogonal ones in the monoclinic structure. Structural models of these interfaces cannot be easily deduced from the HRTEM images. Such interfaces must cause high strains in both structures and cannot be coherent on long distances, thus they are not likely to occur in bulk crystals. A limited occurrence of these relations in nanoparticles can be explained by higher flexibility of their structure.

It should be noted that in all the cases observed in this work the $m \rightarrow t$ transition started at the free surfaces of the particles. Moreover, the (100) planes of the monoclinic phase were the first to become either the (110) (orientation relation 1) or the (001) (orientation relation 3) planes of the tetragonal phase. Considering the surface energies [11] of the planes that form the contour of the particles, one can find that the energy gain $\Delta\gamma_{m(100)\rightarrow\ t(110)}$ = 8.1 %, and $\Delta\gamma_{m(100)\rightarrow\ t\ (001)}$ = 14.0 %. Thus, for nanoscale particles, the orientation relation (3) (1b in Table 1) should be more favourable than the relation (1) (1a in Table 1). Even more energy could be gained if the transition would start at the *m*(111) plane: $\Delta\gamma_{m(111)\rightarrow\ t\ (101)}$ = 19.5 %, but the strain caused by the mismatch between the orthogonal and non-orthogonal lattices in *t*- and *m*-structures inhibited the transition along the *m*[111] direction. Among the other variants, which are compatible with both the conditions *m*[001] || *t*[001] and *m*[010] || *t*[110] and do not involve matching orthogonal and non-orthogonal lattices, one can mention $m(\bar{1}01)\rightarrow t(112)$ and $m(101)\rightarrow t(112)$. Unfortunately, no data is available on the surface energy of the *t*(112) planes. The plane *m*(101) itself has a high surface energy and is not likely to play an important role in the formation of crystallite shape and to initiate the transition. The surface energy of the $m(\bar{1}01)$ plane is considerably lower, but we do not have any evidence of its appearance.

It may be concluded that the mechanism of *t*-ZrO_2 stabilization by small crystallite size due to the lower surface free energy of the tetragonal phase [9] was the one that actually worked for the material studied. The above considerations and the fact that the tetragonal particles observed in this work were, on average, smaller than the monoclinic ones (7.4 nm and 9.2 nm, respectively) confirm that. Adsorption of certain ions on the surfaces of the zirconia particles during their preparation could also act as a factor stabilizing *t*-ZrO_2 [46, 47]. The first $t \rightarrow m$ transition can be attributed to the removal of these adsorbates due to the thermovacuum treatment inside the column of the electron microscope (pressure of $2.5 \cdot 10^{-5}$ Pa and temperature of

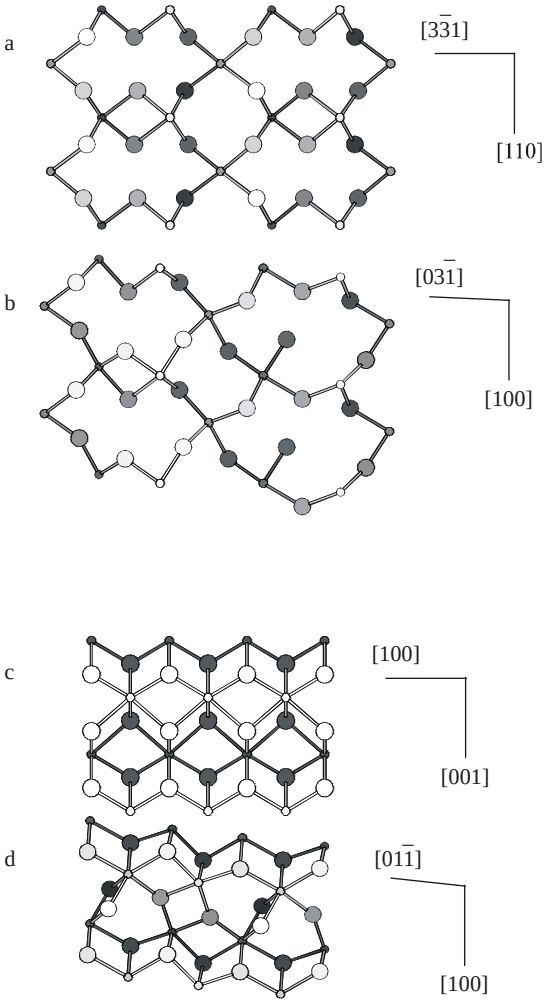

Fig. 7. Lattice planes matched (habit planes) in the case of orientation relations (2) and (4) in the tetragonal (a, c) and monoclinic (b, d) structures of ZrO_2. a) (116) plane of t-ZrO_2; b) (013) plane of m- ZrO_2; c) (010) plane of t-ZrO_2; d) (011) plane of m- ZrO_2. Small circles – Zr, large circles – O; shade shows the depth.

$n \cdot 10^2$ °C). The second transition ($m \rightarrow t$) was observed at higher temperatures, after the electron beam had been concentrated in high-resolution mode. This can be interpreted as the recovery of the structure that was thermodynamically stable for the particles of certain size under the temperature considerably lower than the bulk transition temperature.

5. Conclusion

Monoclinic-to-tetragonal phase transitions within unconstrained nanoparticles of ZrO_2 lead to the following orientation relations between the phases: 1) *m*(100) || *t*(110), *m*[001] || *t*[001]; 2) *m*(013) || *t*(116), *m*[001] || *t*[001]; 3) *m*(100) || *t*(001), *m*[001] || *t*[110]; 4) *m*(011) || *t*(100), *m*[100] || *t*[001]. The relations 1and 3 occur most frequently; the relations 2 and 4 were found only in combination with 1and 3 in the "core-shell" structures. The tetragonal phase nucleates at the free (100) surfaces of the monoclinic particles. During the transition both the phases coexist within a particle; the interface is coherent. The transition is induced by the electron beam and occurs within the region of thermodynamic instability of the bulk tetragonal phase of zirconia. The tetragonal phase is stabilized by small crystallite size due to the lower surface free energy of *t*-ZrO_2.

6. Acknowledgements

The work has been supported by ZEIT-Stiftung, Hamburg, Germany, within the project "Nanochemie für eine zukünftige Automobiltechnik - Möglichkeiten der Optimierung von kupferbasierten Katalysatoren für die onboard Gewinnung von Wasserstoff aus Methanol". The authors are grateful to anonymous Referee whose valuable comments helped us to improve the manuscript greatly.

References

[1] J. P. Breen and J. R. H. Ross, Catalysis Today 51 (1999) 521.
[2] M. Shimokawabe, H. Asakawa and N. Takezawa, Applied Catalysis 59 (1990) 45.
[3] X. M. Song and A. Sayari, Catal. Rev. – Sci. Eng. 38 (1996) 329.
[4] G. D. Yadav and J. J. Nair, Micropor. Mesopor. Mater. 33 (1999) 1.
[5] Molodetsky, A. Navrotsky, M. Paskowitz, V. J. Leppert and H. Risbud, J. Non-Cryst. Solids 262 (2000) 106.
[6] R. Srinivasan, R. De Angelis and B. H. Davis, J. Mater. Res. 1 (1986) 583.
[7] J. Livage, K. Doi and C. Maziers, J. Amer. Ceram. Soc. 51 (1968) 349.
[8] V. N. Filipovich and A. M. Kalinina, Struct. Glass 5 (1965) 44.
[9] R. C. Garvie, J. Phys. Chem. 82 (1978) 218.
[10] H. Holmes, E. Fuller and R. Gammage, J. Phys. Chem. 76 (1972) 527.
[11] Christensen and E. A. Carter, Phys. Rev. B 58 (1998) 8050.
[12] T. Chraska, A. H. King and C. C. Berndt, Mater. Sci. Eng. A 286 (2000) 169.
[13] E. Djurado, P. Bouvier and G. Lucazeau, J. Solid State Chem. 149 (2000) 399.
[14] Y. Murase and E. Kato, J. Amer. Ceram. Soc. 66 (1982) 196.
[15] G. Skandan, C. M. Foster, H. Frase, M. N. Ali, J. C. Parker and H. Hahn, Nanostruct. Mater. 1 (1992) 313.
[16] M. Winterer, R. Nitsche, S. A. T. Redfern, W. W. Schmahl and H. Hahn, Nanostruct. Mater. 5 (1995) 679.
[17] K. T. Jung and A. T. Bell, J. Molecular Catal. A 163 (2000) 27.

[18] J. C. Ray, P. Pramanik and S. Ram, Mater. Lett. 48 (2001) 281.
[19] P. Bouvier, E. Djurado, C. Ritter, A. J. Dianoux and G. Lucazeau, Int. J. Inorg. Mat. 3 (2001) 647.
[20] G. Pacheco and J. J. Fripiat, J. Phys. Chem. B 104 (2000) 11906.
[21] G. K. Chuah, Catalysis Today 49 (1999) 131.
[22] J. C. Ray, R. K. Pati and P. Pramanik, J. Eur. Ceram. Soc. 20 (2000) 1289.
[23] G. Rauchs, T. Fett, D. Munz and R. Oberacker, J. Eur. Ceram. Soc. 21 (2001) 2229.
[24] M. Oskarsson, E. Ahlberg and K. Pettersson, J. Nucl. Mater. 295 (2001) 126.
[25] P. Bouvier, E. Djurado, G. Lucazeau and T. Le Bihan, Phys. Rev. B 62 (2000) 8731.
[26] M. I. Osendi, J. S. Moya, C. J. Serna and J. Soria, J. Amer. Ceram. Soc. 68 (1985) 135.
[27] R. Srinivasan, L. Rice and B. H. Davis, J. Amer. Ceram. Soc. 68 (1990) 135.
[28] T. Mitsuhashi, M. Ichihata and U. Tatsuke, J. Amer. Ceram. Soc. 57 (1974) 97.
[29] N.-L. Wu, T.-F. Wu and I. A. Rusakova, J. Mater. Res. 16 (2000) 666.
[30] D. Simeone, J.L. Bechade, D. Gosset, A. Chevarier, P. Daniel, H. Pilliaire and G. Baldinozzi, J. Nuclear Mater. 281 (2000) 171.
[31] J. E. Bailey, Proc. R. Soc. A279 (1964) 395.
[32] G. M. Wolten, Acta Cryst. 17 (1964) 763.
[33] D. K. Smith and H. W. Newkirk, Acta Cryst. 18 (1965) 983.
[34] R. N. Patil and E. C. Subbarao, Acta Cryst. 26 (1970) 535.
[35] G. K. Bansal and A. H. Heuer, Acta Metall. 22 (1974) 409.
[36] S. T. Buljan, H. A. McKinstry and V. S. Stubican, J. Amer. Ceram. Soc. 59 (1976) 351.
[37] B. C. Muddle and R. H. J. Hannink, J. Amer. Ceram. Soc. 69 (1986) 547.
[38] G. R. Hugo and B. C. Muddle, Mater. Sci. Forum 56-58 (1990) 357.
[39] W. Z. Zhu, T. C. Lei, Y. Zhou and Z. S. Ding, J. Mater. Sci. Letters 15 (1996) 69.
[40] V. Ya. Shevchenko, A. E. Madison and V. B. Glushkova, Glass Phys. Chem. 27 (2001) 400.
[41] V. Ya. Shevchenko, O. L. Khasanov, A. E. Madison and J. Y. Lee, Glass Phys. Chem. 28 (2002) 322.
[42] R. A. Caruso, M. Antonietti, M. Giersig, H.-P. Hentze and J. Jia, Chem. Mater. 13 (2001) 1114.
[43] M. Antonietti, R. A. Caruso, C. G. Göltner and M. C. Weissenberger, Macromolecules 32 (1999) 1383.
[44] H. McMurdie, M. Morris, E. Evans, B. Paretzkin, W. Wong-Ng and C. Hubbard, Powder Diffraction 1 (1986) 275.
[45] L. Lutterotti and P. Scardi, J. Appl. Cryst. 23 (1990) 246.
[46] S. Gutzov, J. Ponahlo, C. L. Lengauer and A. Beran, J. Amer. Ceram. Soc. 77 (1994) 1649.
[47] R. Srinivasan, B. H. Davis, O. Burl Cavin and C. R. Hubbard, J. Amer. Ceram. Soc. 75 (1992) 1217.